PAPER

Check for updates

A versatile test system to determine nanomaterial heteroagglomeration attachment efficiency†

Helene Walch, [iD] ‡[a] Nada Bašić,[a] Antonia Praetorius, [iD][ab] Frank von der Kammer [iD] *[a] and Thilo Hofmann [iD] *[a]

Engineered and incidental nanomaterials are emerging contaminants of environmental concern. In aquatic systems, their transport, fate, and bioavailability strongly depend on heteroagglomeration with natural suspended particulate matter (SPM). Since particulate contaminants are governed by different mechanisms than dissolved contaminants, harmonized, particle-specific test systems and protocols are needed for environmental risk assessment and for the comparability of environmental fate studies. The heteroagglomeration attachment efficiency (α_{het}) can parametrize heteroagglomeration in fate models which inform exposure assessment. It describes the attachment probability upon nanomaterial–SPM collision and reflects the physicochemical affinity between their surfaces. This work introduces a new versatile test system to determine α_{het} under environmentally relevant conditions. The test matrix combines model SPM analogs and an adjustable model hydrochemistry, both designed to represent the process-relevant characteristics of natural freshwater systems, while being standardizable and reproducible. We developed a stirred-batch method that addresses shortcomings of existing strategies for α_{het} determination and conducted heteroagglomeration experiments with CeO_2 (<25 nm) as a model nanomaterial. Single-particle ICP-MS allowed working at environmentally relevant concentrations and determination of α_{het} values by following the decrease of non-reacted nanomaterial over time. The α_{het} values received for the model freshwater test matrix were evaluated against a natural river-water sample. Almost identical α_{het} values show that the model test system adequately reflects the natural system, and the experimental setup proved to be robust and in line with the theoretical concept for α_{het} determination. Combinations of natural SPM in model water and model SPM in natural water allowed further insight into their respective impacts. The α_{het} values determined for nano-CeO_2 in the natural river water sample (0.0044–0.0051) translate to a travel distance of 143–373 km downstream until 50% is heteroagglomerated, assuming an average flow velocity of 5 km h^{-1}, an SPM concentration of 20–45 mg L^{-1}, and experimental mixing conditions (*i.e.*, $G \sim 97$ s^{-1}). These half-lives illustrate the importance of heteroagglomeration kinetics.

Environmental significance

Fate and risk assessment for anthropogenic nanomaterials require dedicated test systems for particulate contaminants. In freshwaters, transport, fate, or bioavailability, for example, strongly depend on nanomaterial heteroagglomeration with suspended particulate matter (SPM), but test systems are not available yet. We demonstrate a new adjustable test system to determine heteroagglomeration attachment efficiencies (α_{het}) under environmentally relevant conditions. The developed model freshwater matrix (SPM analog flocs in a model hydrochemistry) was successfully evaluated against a natural water sample, employing a newly developed stirred-batch method, which addresses shortcomings of existing strategies to determine α_{het}. This approach will enable researchers to study the fate of particulate contaminants under more realistic but well-defined and reproducible laboratory conditions, which is much needed in risk assessment.

[a] *Department of Environmental Geosciences (EDGE), Centre for Microbiology and Environmental Systems Science (CeMESS), University of Vienna, Josef-Holaubek-Platz 2, 1090 Vienna, Austria. E-mail: h.walch@gmx.at, helene.walch@umweltbundesamt.at, nadaibasic@gmail.com, frank.kammer@univie.ac.at, thilo.hofmann@univie.ac.at*
[b] *Department of Ecosystem & Landscape Dynamics, Institute for Biodiversity and Ecosystem Dynamics, University of Amsterdam, Science Park 904, 1098 XH Amsterdam, The Netherlands. E-mail: a.praetorius@uva.nl*
† Electronic supplementary information (ESI) available: Link to SP-ICP-MS particle integration and counting tool: **https://github.com/WalchH/SP-ICP-MS_ particle_integration_counting**. See DOI: **https://doi.org/10.1039/d3en00161j**
‡ Present address: Studies & Consulting, Environment Agency Austria – Laboratories, Spittelauer Lände 5, 1090 Vienna, Austria.

1. Introduction

Nanomaterials (NMs) comprise inorganic, organic, carbonaceous, or composite materials of natural or anthropogenic origins. Anthropogenic NMs are either intentionally produced engineered NMs or incidental NMs arising as by-products from human activity.[1,2] Both receive much scientific and public attention as emerging environmental contaminants.[3] Examples are black carbon, soot, engineered metal- or carbon-based nanomaterials,

588 | *Environ. Sci.: Nano*, 2024, **11**, 588–600

This journal is © The Royal Society of Chemistry 2024

advanced materials, nanoplastics, and (nano-sized fractions of) tire- and brake wear. What they all have in common is that they are particles and have to be treated as such when assessing their behavior, transport, and fate in the environment.[4,5]

Rivers are a relevant compartment for the environmental fate of NMs and constitute potential long-distance transport routes towards marine systems. Unless NMs dissolve or degrade, their transport behavior and fate are governed by their affinity to agglomerate, either with the same particle type (homoagglomeration) or with naturally present suspended particulate matter (SPM) (heteroagglomeration). In natural surface waters, where SPM is omnipresent, heteroagglomeration dominates.[6–9] Heteroagglomeration is crucial for environmental risk assessment as it shifts apparent concentrations of free and attached NMs. This affects their location of action (in the water column or within SPM), their sedimentation behavior, the role of sediments as (intermediate) sinks,[10] and their bioavailability or trophic transfer.[11,12]

For the parametrization of heteroagglomeration in fate models and exposure assessment, the heteroagglomeration attachment efficiency (α_{het}) is considered most suitable.[7,10,13] It describes the probability of attachment upon NM–SPM collision and reflects the physicochemical affinity between NM and SPM under given hydrochemical conditions while being independent of the collision frequency and, thus, the relative NM : SPM concentrations.[14] For homoagglomeration, the OECD test guideline (TG) No. 318 (Dispersion Stability of Nanomaterials in Simulated Environmental Media)[15,16] is available. A harmonized test system to determine α_{het} is still lacking[17,18] and required development of realistic yet generalizable testing conditions.[7]

An ideal setup (1) covers primary heteroagglomeration between NM and SPM while avoiding interferences of homoagglomeration or secondary heteroagglomeration between NM–SPM associations. (2) It allows resolving fast and slow heteroagglomeration (high and low α_{het}), and (3) working at environmentally relevant NM concentrations. (4) It represents the process-relevant characteristics of natural SPM and hydrochemistry while being reproducible, and (5) it allows deriving α_{het} according to agglomeration theory.

Praetorius et al.[7] reviewed available strategies to determine α_{het}, but all approaches fell short on at least one of the above criteria. Many studies used simple SPM analogs,[14,19–23] sometimes in filtered natural water,[24–27] while some employed natural water samples[28] or sludge from wastewater treatment plants.[29] Neither simple analogs nor specific natural samples allow generalizations.

The employed analytical techniques imply weaknesses. For dynamic light scattering (DLS),[19,20,22,23,25–27,30,31] agglomerates may exceed the instrument's size limits, sedimentation may occur and invalidate the assumption of diffusive motion only, and very disparate particle sizes induce bias through stronger scattering of larger particles. With typically much larger SPM than NM, size changes by primary heteroagglomeration are not detectable and only secondary heteroagglomeration induces size increase. This is also true for laser diffractometry (LD) and was part of the theoretical concept to derive α_{het} employing LD.[14,32] A required occurrence of secondary heteroagglomeration complicates resolving slow agglomeration and does not allow working at environmentally relevant NM concentrations (μg to ng L^{-1} (ref. 3 and 33)). Low sensitivities of LD and DLS for small particles require working at elevated NM concentrations. In stirred-batch experiments,[28,34] the non-settling NM fraction was quantified by ICP-OES (inductively coupled plasma optical emission spectrometry), which also attains limited sensitivity. Compensating for low analytical sensitivity by employing high NM concentrations increases the probability of homoagglomeration and impedes resolving the early phase of fast agglomeration processes.

Finally, the theoretical assumptions beyond α_{het} determination do not always reflect the experimental conditions. Retrieving α_{het} by relating slow heteroagglomeration rates (reaction-limited) to fast rates (diffusion-limited, $\alpha_{het} = 1$), for example employing time-resolved DLS, requires resolving initial doublet formation.[35] This is hard to achieve by DLS, especially for fast agglomeration or large size differences between NM and SPM. The assumed agglomeration-breakup equilibrium for deriving α_{het} from batch experiments[21,34] is questionable because deagglomeration is less likely,[36,37] especially concerning the detachment of NMs from complex SPM flocs. What is thought to be free NM in an agglomeration-breakup equilibrium may be an intrinsically stable or matrix-stabilized subpopulation of the NM. NM can also attach or be screened during the separation of free and heteroagglomerated NM by sedimentation or centrifugation (especially at high concentrations). Lastly, the Smoluchowski-based model used with time-resolved LD[14,24,38] works well for simple SPM analogs (e.g., SiO$_2$) but may face its limits if complex SPM flocs are to be parameterized.

In this work, we introduce an adjustable test system to determine α_{het} under environmentally relevant conditions by combining the complex SPM analogs previously developed by the authors[39] with the model water composition suggested in OECD TG 318.[15,16] The SPM analogues were designed to represent those characteristics of natural SPM relevant for agglomeration processes, and the model water composition covers hydrochemical parameters (i.e., pH, electrolytes and NOM), which were selected based on their impact on agglomeration and their prevalence in natural river waters.[15,16] This model freshwater matrix was evaluated against a natural river water sample. CeO$_2$ was used as a model NM. To determine α_{het}, we developed a stirred-batch method addressing the shortcomings of existing methods and meeting the above requirements. The setup allows (1) to investigate and distinguish hetero- and homoagglomeration processes through controls and complementary measurements, (2) to work at environmentally relevant concentrations with single-particle ICP-MS, a sensitive and particle-specific analytical technique,

This journal is © The Royal Society of Chemistry 2024

Environ. Sci.: Nano, 2024, 11, 588–600 | 589

(3) to resolve fast and slow agglomeration processes by playing with concentrations and experiment duration, and (4) to derive α_{het} in accordance with agglomeration theory. The proposed model freshwater matrix and experimental protocol will support research and regulation employing α_{het} as a NM fate descriptor. Sensitive analytical techniques for organic NMs like nanoplastics still need to be developed, but test principles are equally applicable.

2. Experimental

2.1. Materials

Natural SPM stock. River water (Danube Channel, Vienna, AT) was collected close to the surface in July 2020 in 5 L containers (PETG, Nalgene Biotainer, ThermoFisher), and processed in the lab within two days. The water was passed through a 125 μm steel mesh to remove coarse grains and plant parts. Initial SPM size (see S4†) was measured by time-resolved LD for at least one hour in a sample aliquot of 1.5 L, as described previously.[39] SPM was concentrated by repeated centrifugation (14 min, 4200 rpm, 5897 g, Cryofuge 6000i, Heraeus, see S5†) and removal of the supernatant by slow suction from the top, employing a glass pipette and vacuum pump. The SPM mass concentration in the concentrated stock was 12.1 ± 0.09 g L^{-1}, gravimetrically determined in triplicates by depositing 0.8 mL dropwise onto pre-weighed filters (0.02 μm pore size, 25 mm diameter, Anodisc, Whatman), employing a vacuum filtration unit, and drying them at 55 °C. The concentrated stock was sterilized by adding NaN$_3$ at 200 mg L^{-1} and stored in the dark at 4 °C until usage.

Natural river water. The supernatant collected during natural SPM stock preparation was filtered through a hollow fiber filter unit (0.05 μm, polysulfone, MidiKros TC, Spectrum, Repligen) to remove microorganisms and remnant fine particles before storage in the dark at 4 °C (PETG Nalgene Biotainer, ThermoFisher). Cation concentrations were determined in acidified samples by ICP-OES (5110, Agilent Technologies) and anions by ion chromatography (ICS-1000, Dionex). Dissolved organic carbon (DOC), as non-purgeable organic carbon (NPOC) after acidification, and total dissolved nitrogen (TDN) were determined with a TOC analyzer (TOC-L, Shimadzu). Relevant characterization data are given in Table 1 (more details in S1†).

Model SPM stock. SPM analogs were prepared by flocculation in a stirred-batch setup according to the procedure described in Walch et al.[39] Briefly, stock suspensions of illite (prepared from rock chips of IMt-2, The Clay Minerals Society), quartz (prepared from SiO$_2$ powder, 0.5 μm, Alfa Aesar), hematite (prepared by forced hydrolysis according to Wang

et al.[40]), and tryptophan (prepared from L-tryptophan powder, ≥98%, Sigma Aldrich) were mixed to reach final concentrations of 18.83, 23.02, 3.15 and 3.48 mg L^{-1}, respectively. The latter corresponds to a carbon concentration of 2.25 mg L^{-1}. Starting from quartz and illite in HCl-acidified ultrapure water (pH ∼ 5), hematite and tryptophan (each diluted in 100 mL acidified water right before addition) were quickly added to the stirred batches in the given sequence, reaching a final volume of 0.8 L per batch and a total mineral mass concentration of 45 mg L^{-1}. The pH was adjusted to 5 and floc formation and stabilization were followed by time-resolved LD (Mastersizer 2000, Malvern). Batches were left in the dark at 4 °C for sedimentation (>48 h, until the supernatant had cleared). The supernatant was carefully removed by suction from the top, noting the remaining weight to calculate the SPM concentration in the stock. Stocks were prepared freshly, max. one week before an experiment, and stored in the dark at 4 °C.

River water analog (model water). River water analog was prepared based on the *alternative medium* in OECD TG 318.[15] CaCl$_2$, MgSO$_4$ and MgCl$_2$ salts were added to ultrapure water to adjust Ca^{2+}, Mg^{2+} and SO$_4^{2-}$ concentrations to the values measured in natural river water (Table 1). Since Cl$^-$ is more abundant in river waters,[41] chloride salts were used instead of nitrate salts recommended in the guideline. DOC was adjusted with dissolved Suwannee River natural organic matter (SR-NOM, 2R101N, International Humic Substances Society), prepared according to OECD TG 318.[15] SR-NOM carbon contents, determined from three stock preparations on the TOC analyzer (as above), were 38.2 ± 1.9%$_{wt}$, in accordance with expected values (42.6%$_{wt}$,[42] 46.2%$_{wt}$ (ref. 43)). The pH was adjusted to 8.3 and maintained during experiments by adding 0.1 mmol L^{-1} NaOH.

CeO$_2$ NM stock and spiking suspensions. NM stock was prepared dispersing 98 mg of CeO$_2$ powder (<25 nm, Sigma Aldrich) in 5 mL acidified ultrapure water (pH 5) using an ultrasonic vial tweeter (UP 2000St and S26d11x10, Hielscher), yielding a stock concentration of 19.6 g L^{-1}. NM characterization data is given in S2.† Spiking suspensions for agglomeration experiments were prepared just before spiking by a two-step dilution of the NM stock in acidified ultrapure water (pH ∼ 5) to a final concentration of 7.5 mg L^{-1}.

2.2. Methods

SPM suspension preparation & characterization. For heteroagglomeration experiments, four test systems combining natural SPM (nat.SPM) and model SPM (mod.

Table 1 Natural river water characterization

| pH | Cations [mmol L^{-1}] | | | Anions [mmol L^{-1}] | | DOC [mg L^{-1}] |
	Ca^{2+}	Mg^{2+}	Na^{2+}	SO$_4^{2-}$	Cl$^-$	
8.3	1.118	0.414	0.314	0.238	0.319	2.52

Fig. 1 Schematic overview on sample preparation procedure and resulting model, natural and combined test systems.

SPM) in natural water (nat.W) and model water (mod.W) were used (Fig. 1), and two final concentrations of SPM (45 and 20 mg L^{-1}). Suspensions were prepared at 45 mg L^{-1} from concentrated SPM stocks the day before the experiment. The total suspension volume of 1.6 L was split into two bottles (1 L PP centrifuge bottles with sealing screw cap, Heraeus) and left on an overhead shaker (16 rpm, Reax 20/8, Heidolph) overnight to precondition flocs in the respective hydrochemistry. Natural SPM suspensions were sonicated (40 W, 10 min, TT13 tip, Sonoplus 3200, Bandelin) before shaking, to break up any clumps formed by centrifugation during stock preparation. For experiments at 20 mg L^{-1} SPM, suspensions were further diluted with mod.W or nat.W. Before starting an experiment, suspensions were stabilized under experimental stirring conditions (see S3†) for at least one hour, recording SPM floc sizes and fractal dimensions by LD (Mastersizer 2000, Malvern) as described before.[39] Further floc characterization included zeta potential (ZP) measurements and scanning electron microscopy (SEM) imaging. Data is compiled in S4.†

Heteroagglomeration experiments. For heteroagglomeration experiments, two stirred batch reactors (see S3†) were operated simultaneously at a fill level of 750 mL SPM suspension and an average shear rate (G) of ~97 s^{-1} (see S8†). Blank samples were taken from each batch before adding 0.5 mL NM spiking suspension to reach a final NM concentration of 5 μg L^{-1}. To establish NM removal curves, sampling proceeded at increasing intervals noting the sampling time (over periods of 6.4 ± 1.5 h for experiments at 20 mg L^{-1} SPM and 22 ± 3 h for experiments at 45 mg L^{-1} SPM). For the blanks, and at each of the 9 sampling occasions, triplicates of 3 mL and 0.8 mL were sampled from the surface of each batch and pipetted into centrifuge tubes (15 mL, metal-free, Carl

Roth). The removed volume was not replaced. The 3 mL samples were put aside for total digestion and ICP-MS measurement to control for mass losses. Tubes receiving the 0.8 mL samples were prefilled with 5.2 mL ultrapure water, diluting the sample instantly to inhibit further agglomeration and to avoid NM screening by sedimenting SPM during subsequent centrifugation (see S5†). They were immediately centrifuged (6 min, 4500 rpm, 4166 g, CR 4.22, Jouan) to separate heteroagglomerated from free NM (see S5†), and 3 mL of the supernatants were sampled at a fixed depth (slightly below the 3 mL tube mark) employing an electronic pipette (100–5000 μL Research pro, Eppendorf) mounted on a stand. The supernatants were transferred into tubes prefilled with 3 mL ultrapure water (total dilution factor 1:15) and analyzed by SP-ICP-MS as fast as possible to determine NM particle number concentrations and sizes. The size gives insight into potentially co-occurring homoagglomeration; the particle number concentration quantifies the non-heteroagglomerated NM fraction remaining in suspension.

Homoagglomeration control. Controls were run in duplicates in nat.W and mod.W without SPM to assess the impact of homoagglomeration on NM removal from suspension. Experiments were conducted analogously to heteroagglomeration experiments with few adjustments: for blanks, and at each sampling time, 6 mL were sampled and centrifuged undiluted (as screening is negligible in the absence of larger SPM). Of the 3 mL supernatant sampled, 1 mL was transferred into tubes prefilled with 14 mL ultrapure water (dilution factor 1:15) for SP-ICP-MS analysis of NM particle numbers and sizes. To close the mass balance, the remaining 2 mL supernatant and the 3 mL remaining at the bottom after centrifugation were digested and analyzed by ICP-MS.

This journal is © The Royal Society of Chemistry 2024

Environ. Sci.: Nano, 2024, **11**, 588–600 | **591**

SP-ICP-MS analysis. The diluted (1:15) supernatants were immediately analyzed for ^{140}Ce on ICP-MS (7900, Agilent, equipped with an ISIS3 introduction system and ASX-500 autosampler), operated in time-resolved analysis (TRA) mode (sample flow 0.346 mL min^{-1}, dwell-time 0.1 ms, measurement time 60 s). To allow the determination of NM equivalent spherical diameters from SP-ICP-MS data, calibrations for Ce and Au (analyzed for ^{197}Au) were done with dissolved elemental standards (diluted from 1 g L^{-1}, Inorganic Ventures), and Au particle standards (30 nm, BBI Solutions) were used to determine transport efficiency. For quantification and sizing of NM particles, three or more signals in a row ≥ 3 counts (background cut-off determined as described in S6†) were counted as particle events. The particle number concentration in the sample was determined dividing the particle events in one minute measurement time by the sample introduction flow (determined with TruFlow meter, Nordson) and the total dilution factor (1:15). Particle sizes were derived as described in S7.†

Digestion and ICP-MS analysis. CeO$_2$ NM was digested adding 1 part of HNO$_3$ (65%, Suprapur, Merck Millipore, twice subboiled) and 1 part of H$_2$O$_2$ (30%, Suprapur, Merck Millipore) to 3 parts of sample. The tubes were closed and left in a heated ultrasonic bath (80 °C, 160 W effective ultrasonic power, Elmasonic X-tra 50 H, Elma) for minimum 5 h. Before measurement, 10 parts of ultrapure water were added to cooled digests (total sample dilution factor 0.2). Samples were analyzed for ^{140}Ce on ICP-MS operated in spectrum mode (stabilization time 8 s, integration time 0.1 s, Ce calibration levels 0.005, 0.025, 0.05, 0.25, 0.5, 5, 50 µg L^{-1} in 4% HNO$_3$).

Attachment efficiency determination. NM removal curves were used to determine the heteroagglomeration attachment efficiency (α_{het}) based on Smoluchowski's agglomeration theory. If a constant number concentration of SPM flocs is assumed, removal of NM due to heteroagglomeration proceeds at a pseudo-first-order rate (Equation 1).[44]

Equation 1. Pseudo-first-order rate law for nanomaterial (NM) removal.

$$\frac{dn_{NM}}{dt} = -k^*_{het} n_{NM}$$

n_{NM}	Nanomaterial number concentration [m^{-3}]
t	Time [s]
k^*_{het}	Pseudo 1st order heteroagglomeration rate constant [m^3 s^{-1}]

Consequently, the logarithm of the NM number concentration (n_{NM}) plotted over time yields a linear relation with a slope equaling the pseudo-first-order heteroagglomeration rate constant (k^*_{het}). The heteroagglomeration attachment efficiency (α_{het}) was derived from the initial slope, representing early (primary) agglomeration, employing Equation 2. The required SPM number concentrations (n_{SPM}) were approximated from SPM mass concentrations in two ways, either employing the

particle-number-based mode SPM diameter or the particle-number-based SPM size distribution, and heteroagglomeration collision rate constants ($k_{coll,het}$) were calculated for both cases. See S8† for details.

Equation 2. Pseudo-first-order heteroagglomeration rate constant.

$$k^*_{het} = -k_{coll,het} n_{SPM} \alpha_{het}$$

$k_{coll,het}$	Heteroagglomeration collision rate constant [m^3 s^{-1}]
α_{het}	Heteroagglomeration attachment efficiency [–]
n_{SPM}	SPM number concentration [m^{-3}]

3. Results and discussion

Heteroagglomeration between CeO$_2$ NM and SPM was observed in all four test systems (Fig. 2). The fastest NM removal occurred in the mod.SPM–nat.W combination. The other test systems exhibited a slower removal and behaved more similarly to each other.

3.1. Model system reflects natural system

The determined heteroagglomeration attachment efficiencies (α_{het}) for the model system (mod.SPM–mod.W) were well aligned with the natural system (nat.SPM–nat.W) (Fig. 3), showing that the model system reflects the process-relevant characteristics of the natural sample. At 45 mg L^{-1} SPM, α_{het} ranges were 0.0016–0.0025 and 0.0015–0.0054, for the model and natural system respectively. That range comprises α_{het} values derived using the number-based mode SPM diameter ($\alpha_{het\_nr-mode}$) and the SPM size distribution ($\alpha_{het\_size-dis}$) (see S8†). As the nat.SPM–mod.W combination exhibited slightly lower α_{het} values (0.0090–0.0023), the model system ranks between nat.SPM–nat.W and nat.SPM–mod.W.

With the highest values for the mod.SPM–nat.W combination, all determined α_{het} values spanned two orders of magnitude (0.0009–0.09). In pre-experiments with mod. SPM in rather favorable mod.W compositions, $\alpha_{het\_nr-mode}$ values between 0.5 and 0.6 were measured. This confirms that the method is applicable for the α_{het} range in which heteroagglomeration is relevant. According to modelling results from Meesters et al.,[10] heteroagglomeration and co-transport of NMs with SPM play a role at α_{het} between 0.0001–1, and lower α_{het} values justify the assumption that the heteroagglomerated NM fraction is negligible.

Our α_{het} values are within the range of those reported for TiO$_2$ NM (0.8 mg L^{-1}) and SiO$_2$ (100 mg L^{-1}) as a model SPM[14] in hydrochemical conditions closest to the present study. Those were pH 8 and 1 or 10 mg L^{-1} Suwannee River humic acid plus 100 mmol L^{-1} NaCl (α_{het} = 0.02 and <0.001) or 5 mmol L^{-1} CaCl$_2$ (α_{het} = 0.3 and 0.2). Barton et al.[34] also reported α_{het} values in that range (0.01 to 0.0003 for different NMs, 0.001 to 0.009 for CeO$_2$) at NM concentrations of 10 or 50 mg L^{-1} in the presence of 3.8 g L^{-1} sewage sludge (pH 7.2, no further information on SPM properties or hydrochemistry). However, a direct comparability of α_{het} values is impeded by different

592 | Environ. Sci.: Nano, 2024, 11, 588–600

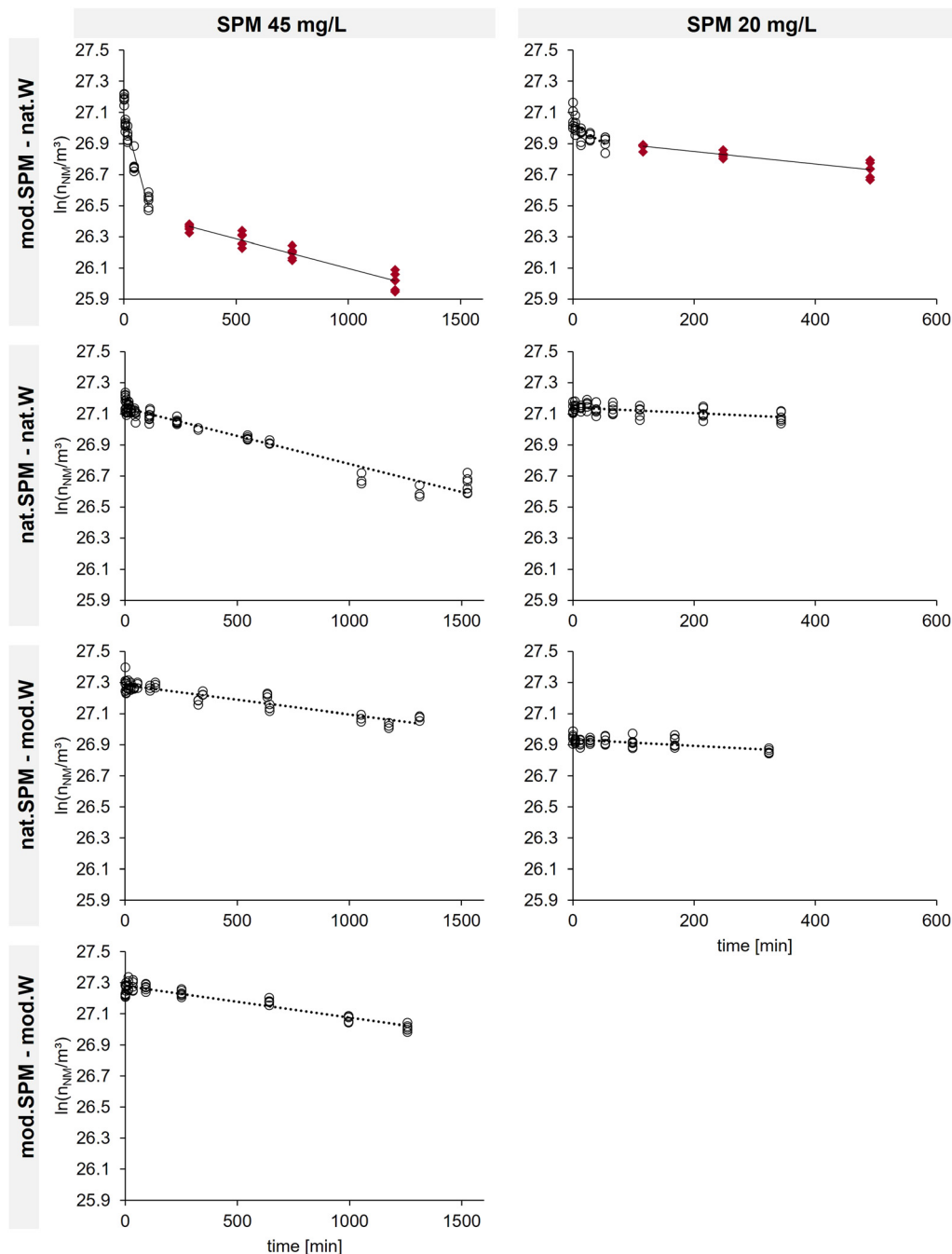This journal is © The Royal Society of Chemistry 2024

Fig. 2 Logarithmized number concentrations of NM remaining in suspension plotted over time for experiments with 45 and 20 mg L^{-1} SPM and different combinations of model flocs (mod.SPM) and natural flocs (nat.SPM) in natural (nat.W) and model water (mod.W). Initial linear slopes (black circles) equal the pseudo-first-order rate constant (k_{het}^*), from which the heteroagglomeration attachment efficiency (α_{het}) was derived. Red diamonds mark a flattening of the slope for the mod.SPM–nat.W combination, which could indicate distinct mechanisms at different agglomeration stages (see 3.3).

theoretical concepts, test matrices (SPM, NM, and hydrochemistry), and methods employed.

3.2. Attachment efficiencies are concentration independent

Both SPM concentrations yielded almost identical α_{het} values (Fig. 3), showing that the method allows determining

concentration-independent attachment efficiencies, suitable for application in environmental fate models.[7,14] Only the nat.SPM–mod.W system, which yielded the lowest α_{het} values of all tested combinations, exhibited higher α_{het} values for the 20 *versus* the 45 mg L^{-1} SPM concentration. This might be due to the shorter experiment duration (300–500 min) at 20 mg L^{-1} SPM. The time span for

This journal is © The Royal Society of Chemistry 2024

Environ. Sci.: Nano, 2024, **11**, 588–600 | **593**
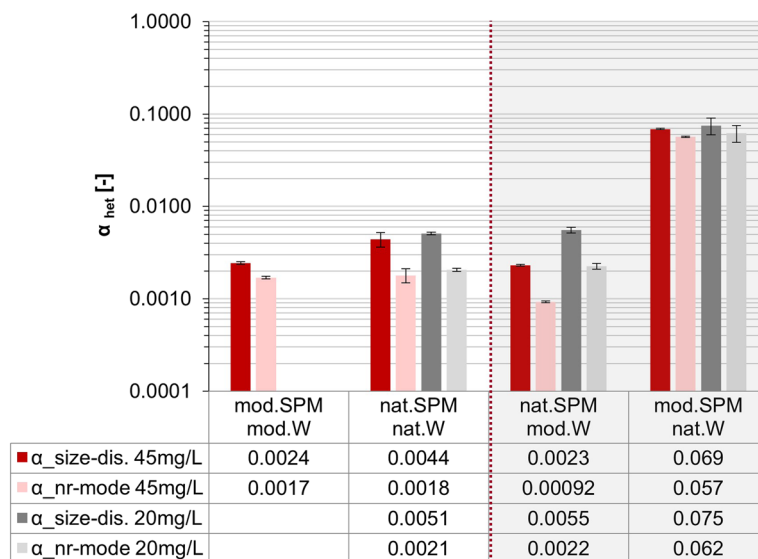
Fig. 3 Heteroagglomeration attachment efficiencies (α_{het}) determined employing either the number-based SPM size distribution (dark red and grey bars) or the mode SPM diameter (light red and grey bars) for experiments carried out at 45 mg L^{-1} SPM (reddish bars) or 20 mg L^{-1} SPM concentrations (greyish bars) with different combinations of model flocs (mod.SPM) and natural flocs (nat.SPM) in model water (mod.W) and natural water (nat.W). Error bars indicate minimum and maximum values for 2 replicates (or 3, in the case of nat.SPM–nat.W at 45 mg L^{-1} SPM). Values in the table represent averages.

experiments with 45 mg L^{-1} SPM was extended to 1200–1500 min, which allowed a more accurate determination of low α_{het} values (Fig. 2). Concentration independence confirms the validity of the theoretical concept and the accuracy of the assumptions for the calculation of $k_{coll,het}$ and n_{SPM} (see S8†).

Applying SPM size distributions *versus* SPM number-mode diameters to calculate $k_{coll,het}$ and n_{SPM} leads to more pronounced deviations of α_{het} values. A sensitivity analysis (given in S9†) shows that $\alpha_{het\_size-dis}$ values are more robust to changes in parameters involved in α_{het} derivation than $\alpha_{het\_nr-mode}$ values. This is due to an enhanced accuracy of SPM size, which strongly impacts the calculated $k_{coll,het}$ and n_{SPM}.

3.3. Hydrochemistry has a stronger impact on α_{het} than SPM-type

The α_{het} values at 45 mg L^{-1} SPM rank mod.SPM–nat.W $\gg$ nat.SPM–nat.W $\geq$ mod.SPM–mod.W $\geq$ nat.SPM–mod.W (Fig. 3). This identifies model water as less favorable for heteroagglomeration than natural water and natural SPM as less favorable than model SPM, with hydrochemistry dominating the effect. Apparently, SR-NOM in mod.W attenuated the agglomeration-promoting surface properties of mod.SPM, yielding a model system that adequately reflects the natural system. Hydrochemical impacts are probably related to different NOM characteristics since other relevant parameters (electrolyte ion types/concentrations, pH value, and organic carbon concentration) were consistent between model and natural waters. Adam *et al.*[24] observed a reduced agglomeration of TiO$_2$ upon addition of SR-fulvic acid to

filtered river water and also attributed this to different NOM characteristics.

Natural river water was collected in summer and, despite a previous rain event, low C/N ratios (4.5 for raw river water and ~3 for the final filtered nat.W, given as NPOC/TDN) indicate a significant contribution of microbial extracellular polymeric substances (EPS) to the riverine NOM composition.[45] EPS comprise a mix of molecules with diverse physicochemical properties and favor agglomeration through heterogeneities in charge or hydrophobicity and/or through bridging interactions by large molecules.[45] The SR-NOM in mod.W exhibited a high C/N ratio of 43 (in accordance with Green *et al.*[46]). It mainly consists of small molecules[47,48] (*i.e.*, <10 kDa, with a number-average molecular weight of 1.52 kDa (ref. 49)) with a high density of negatively charged carboxyl groups (pK_a ~ 3)[50,51] that favor electrostatic stabilization of NM (see S2†).

The mod.SPM–nat.W system favored heteroagglomeration, with an α_{het} value one order of magnitude higher (*i.e.*, 0.056–0.070) compared to other combinations (Fig. 3). A quick removal of NM yielded a steep initial slope in the ln(n_{NM})-over-time plot, which flattened later on (Fig. 2). This was not observed for the other test systems. Calculating α_{het} values for later-stage agglomeration (2nd slope in Fig. 2) yields a range of 0.0037–0.016 (comprising $\alpha_{het\_nr-mode}$ and $\alpha_{het\_size-dis}$ for both SPM concentrations). The two slopes indicate different mechanisms at different stages. Model flocs were designed to exhibit heterogeneous physicochemical surface properties that favor agglomeration,[39] and a favorable NOM composition in nat.W further promotes NM removal. Model flocs may have offered more favorable interaction sites (*e.g.*,

594 | *Environ. Sci.: Nano*, 2024, **11**, 588–600

This journal is © The Royal Society of Chemistry 2024

hydroxyl-groups on hematite or illite edges) adsorbing nat. W NOM molecules (EPS) during overnight preconditioning. Initial NM removal may have been governed by pristine or patchily NOM-coated NM surfaces favorably interacting with preconditioned model flocs (e.g., via NOM bridging or electrostatic patches). A depletion of favorable interaction sites on mod.SPM and/or a decreased NM reactivity due to proceeding NOM-stabilization may have slowed agglomeration over time. Later stage α_{het} values are similar to nat.SPM–nat.W but still slightly higher than for nat.SPM and mod.SPM in mod.W (Fig. 3), indicating that hydrochemistry governs later-stage agglomeration and SPM type has less impact. This supports the promotive role of mod.SPM surface during initial agglomeration. Additionally, secondary heteroagglomeration at later stages cannot be excluded and may reduce NM removal due to fewer collisions at lower SPM numbers (cf. S9†). Slower removal with time was also observed for various NMs interacting with sewage sludge.[34] Since the microbial activity in sludge is very high, EPS may have played a role as well. The authors suggested an increasing importance of agglomerate breakup (NM detachment) or modifications to heteroagglomerate chemistry. The latter seems unlikely at high SPM:NM concentration and size ratios, and detachment of NM from complex flocs is improbable.[36,37]

3.4. Homoagglomeration is negligible

Homoagglomeration control experiments showed up to 10% NM removal in nat.W within the first hour (Fig. 4a), but homoagglomeration was not the reason. The decreasing particle number in the supernatants can be attributed to losses to vessel or stirrer surfaces, confirmed by a decreasing total Ce mass recovery within the system, as analyzed by ICP-MS in digested samples (Fig. 4b). Neither NM removal in the supernatant nor total Ce mass-losses were observed in mod. W (Fig. 4a and b). The Ce mass balance (see S10†) indicates preferential losses of larger/heavier NM particles over time in nat.W. Ce mass concentrations in supernatants (see S10†) and NM particle sizes determined by SP-ICP-MS (Fig. 4c) were constant over time in nat.W and mod.W, further excluding homoagglomeration.

Homoagglomeration did not co-occur in heteroagglomeration experiments, as constant NM particle sizes and total Ce mass recoveries over time show (see S11†). The high SPM surface area probably reduced the chance for NM collisions with vessel or stirrer surfaces, inhibiting Ce mass losses that occurred in nat.W homoagglomeration experiments. In literature, homoagglomeration is frequently presumed less relevant than heteroagglomeration in the environment due to a much higher abundance of SPM than NM particles.[14,52–54] Of course, a higher abundance of SPM supports heteroagglomeration, but in our experiments, NM outnumbered SPM by about 1–3 orders of magnitude (depending on whether number-based size distributions or mode sizes are used to calculate NM or SPM numbers, see S9†). At environmentally relevant mass concentrations of NM and SPM, it is possible that NM numbers exceed those of SPM (see S10†). The dominance of heteroagglomeration in that case results from typically much larger sizes of SPM than NM: since the relative sizes of NM and SPM strongly influence the collision frequency (see the equation for $k_{coll,het}$ in S8†).

Model calculations simulating our experiments based on Smoluchowski's agglomeration theory (S10†) show that at 45 mg L^{-1} SPM concentration, heteroagglomeration dominates homoagglomeration unless the attachment efficiency for homoagglomeration (α_{hom}) is higher than α_{het}. A factor 2 higher α_{hom} would yield similar homo- and heteroagglomeration NM removal rates for early-stage agglomeration. Halving the SPM concentration, doubling the NM concentration, reducing stirring speed by two thirds, or reducing the SPM diameter by one fourth at $\alpha_{het} = \alpha_{hom}$ would have the same effect. Since every successful attachment removes two NM particles by homoagglomeration and one by heteroagglomeration, heteroagglomeration would dominate again at later stages. In case of a high α_{hom}, increasing the SPM concentration or reducing the NM
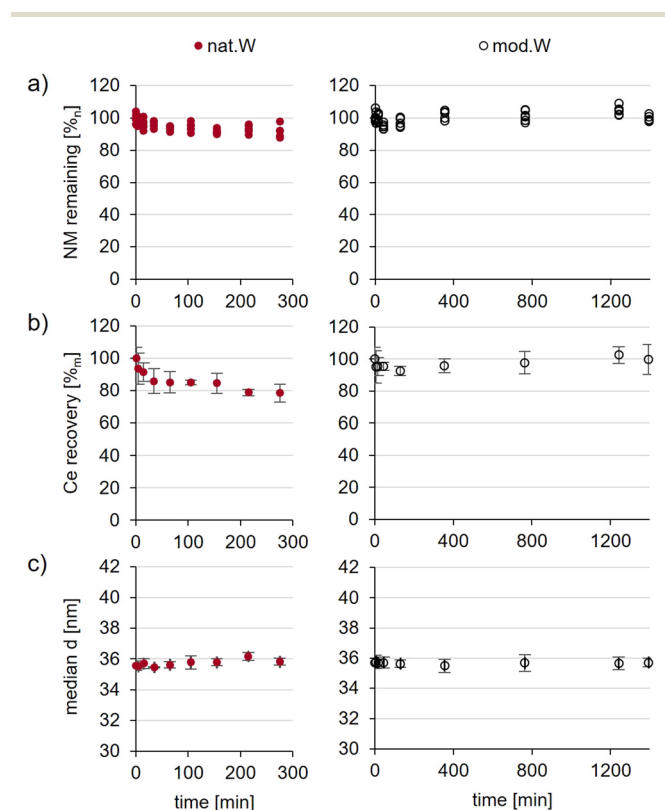

Fig. 4 Homoagglomeration control experiments in natural water (nat. W) and model water (mod.W). a) NM particle number fraction remaining in supernatants analyzed by SP-ICP-MS after centrifugation. b) Total Ce mass recovery in control samples analyzed by ICP-MS after digestion. c) Median equivalent spherical NM diameters as determined from SP-ICP-MS data. Error bars represent standard deviations of $n = 6$ (three subsamples per batch in two batches). Note the different total experiment durations for nat.W and mod.W.
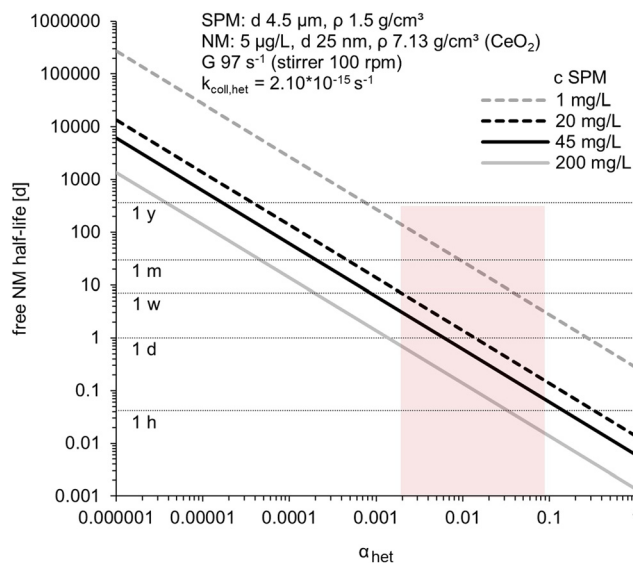
This journal is © The Royal Society of Chemistry 2024

Environ. Sci.: Nano, 2024, 11, 588–600 | 595

Fig. 5 Pseudo-first-order free NM half-life in dependence of α_{het} calculated for different SPM concentrations (c SPM: 1, 20, 45, 200 mg L^{-1}) setting the parameters to represent the experiments (*i.e.*, for SPM: diameter 4.5 μm, density 1.5 g cm^{-3}; for NM: concentration 5 μg L^{-1}, diameter 25 nm, density of CeO$_2$ 7.13 g cm^{-3}; assuming spherical shape for both; velocity gradient G 97 s^{-1} for 100 rpm stirring). Black lines indicate the SPM concentrations used in the experiments, and the shaded area highlights the range of $\alpha_{het\_size\text{-}dis}$ values determined (see Fig. 3).

concentration (with attention to the analytical limits) is thus most effective to avoid interference of homoagglomeration. Alternatively, α_{hom} can be determined from homoagglomeration control experiments and may be used to correct heteroagglomeration NM removal rates. This does not take into account the competition between both processes in the heteroagglomeration setup.

3.5. Heteroagglomeration in freshwaters is not necessarily a fast process

Half-lives for the pseudo-first-order heteroagglomeration reaction help to evaluate the determined α_{het} values (Fig. 5) and were calculated for experimental conditions (see S12†).

Natural flocs in natural water yielded average $\alpha_{het\_size\text{-}dis}$ values of 0.0044 and 0.0051 (Fig. 3), translating to half-lives of 1.2–3.1 days. In a moderately fast river with an average flow velocity of 5 km h^{-1},[55] these half-lives translate to a travel distance of 143–373 km downstream until 50% of the CeO$_2$ NM heteroagglomerated. This is valid if similar water chemistry, SPM concentration, and turbulence, prevail downstream. The SPM concentration in the unprocessed river water sample (53 mg L^{-1}) was actually similar to the experimental concentration (45 mg L^{-1}), but SPM concentrations, sizes, and flow conditions are spatially and temporally highly variable. The turbulence ($G \sim 97$ s^{-1}) in our batch-setup would relate to rather fast flowing upper reaches of rivers,[56] in low-land streams or estuaries G values are usually between <1 and 40 s^{-1}.[57–60] Still, unreacted NM may

be available to organisms over a considerable flow distance and undergo long-range transport as slow heteroagglomeration reduces the chance for deposition by sedimentation.

The highest $\alpha_{het\_size\text{-}dis}$ values (for the mod.SPM–nat.W combination) yield half-lives of only 2 to <5 h, translating to 10–24 km downstream transport at 5 km h^{-1}. This test system was most dissimilar from our natural reference system (nat. SPM–nat.W), but may be relevant for different environmental conditions.

Assuming high SPM concentrations of 200 mg L^{-1} (Fig. 5), α_{het} values ≤0.001 would be required to allow half-lives >1 d. Low SPM concentrations of 1 mg L^{-1} (Fig. 5) would yield half-lives of ±2 months for nat.SPM–nat.W $\alpha_{het\_size\text{-}dis}$ values. Waters with low SPM concentrations and/or unfavorable hydrochemistry (*i.e.*, low α_{het} values) are thus the relevant cases where unreacted NM persists over a significant period of time.

4. Conclusions

We demonstrated a versatile, adjustable model freshwater test system to determine heteroagglomeration attachment efficiencies (α_{het}) for (nano)particulate contaminants. This system is based on an in-depth review of freshwater suspended particulate matter (SPM) and critical components in floc formation,[45] the development of a robust protocol to generate model SPM flocs,[39] and the use of synthetic model freshwater with agglomeration-relevant composition.[61]

Heteroagglomeration attachment efficiencies for CeO$_2$ nanomaterial (NM) were determined in the (adjusted) model test system and the corresponding natural river water sample. The α_{het} values obtained are almost identical, showing that the model system well reflects the process-relevant characteristics of the natural sample.

Model and natural SPM can be transferred into model and natural waters and remain stable. The resulting combined test systems (nat.SPM–mod.W and mod.SPM–nat.W) allow insight into the impacts of SPM and water type on α_{het}, and showed that NOM characteristics may govern heteroagglomeration kinetics. This emphasizes the fact that α_{het} values determined in natural samples only represent this unique situation and cannot be generalized, but the model system allows to compare NMs in a standardized way. Experiments with the same NM in different, well characterized natural samples can help clarify the impact of spatially and seasonally variable NOM characteristics and allows conclusions on specific ecosystems. For example, the α_{het} values for CeO$_2$ in the processed natural sample (nat. SPM–nat.W) yield half-lives of about 1–3 days. This appears short but, employing an average flow velocity of 5 km h^{-1} for moderately fast rivers, translates to 143–373 km translocation downstream until 50% NM heteroagglomerated.

For the given conditions heteroagglomeration is not very fast, indicating that NMs can be quite mobile and bioavailable as single particles.

596 | *Environ. Sci.: Nano*, 2024, **11**, 588–600

This journal is © The Royal Society of Chemistry 2024

The developed stirred-batch method combined with a sensitive analytical technique like (SP)-ICP-MS addresses shortcomings of previous strategies to determine α_{het}, primarily allowing to work at environmentally relevant NM concentrations (in the low µg L^{-1} range) and at realistic NM : SPM concentration ratios. With SPM concentration and size being much larger than that of NM, heteroagglomeration will prevail over homoagglomeration even at almost equal homo- and heteroagglomeration attachment efficiencies. Co-occurring homoagglomeration becomes negligible for attachment efficiencies (α_{hom}) of about one order of magnitude below α_{het}. Homoagglomeration control experiments, NM size determinations, NM mass balances, and NM recoveries help rule out or correct for co-occurring homoagglomeration or NM mass losses to vessel walls or stirrers.

Since α_{het} determination was shown to be almost independent of SPM concentration, the resolution of slow and fast agglomeration processes (high and low α_{het}) can be optimized by modifying SPM concentration and/or experiment duration. Concentration independence moreover implies that the employed theoretical concept and the assumptions on parameters to calculate $k_{coll,het}$ and n_{SPM} were reasonably accurate. Fine-tuning these parameters (e.g., SPM density or the velocity gradient in the batch) may eliminate residual apparent concentration effects on α_{het}.

To resolve primary NM–SPM attachment, early phases of NM removal should be used for α_{het} determination. Secondary heteroagglomeration may occur at later stages, and changes in SPM number and size through floc rupture or growth cannot be excluded, although preconditioning by overnight shaking should stabilize floc size in the respective hydrochemistry. The NM surface properties may also change over time. In the present system, it is likely that an initial eco-corona is formed quickly upon addition of NM for two reasons: (1) the complex composition of NOM from natural water and SR-NOM probably comprises a fraction of molecules with a high affinity for NM surfaces, and (2) environmentally relevant low NM concentrations allow for high NOM : NM ratios. Under these conditions it is unlikely, that pristine NM particles persist long enough to significantly impact heteroagglomeration rates. However, surface coatings may change over time, e.g., thermodynamically favored larger aliphatic or more aromatic fractions of NOM were reported slowly replace kinetically favored smaller and more hydrophilic fractions over time.[62,63] Similarly, engineered NM surface coatings may be slowly replaced by NOM over time.[64] Effects on α_{het} could be studied employing NMs preconditioned in the respective hydrochemistry but may be complicated if this prompts homoagglomeration.

Analysis by SP-ICP-MS is preferable for most inorganic NMs. In addition to low detection limits, operation in single-particle mode allows direct determination of NM number concentrations, particle sizes, and distinction of particles from the potential dissolved background. Digestion and mass-based ICP-MS analysis work too, but require additional sample preparation and dissolved background correction. Moreover, large particles may bias mass-based data in case of polydisperse NM. Multi-element analysis by SP-ICP-TOF-MS can be useful for composite NMs or mixtures of different NMs, and additionally allows differentiation from natural materials through elemental fingerprinting.[65] For organic materials like plastics, selective and sensitive routine analytical techniques still need to be developed or require workarounds like metal-doped particles,[66] but the test principles are equally applicable.

The described test system constitutes a missing link to establish α_{het} as a fate parameter because it enables α_{het} determination under adjustable, environmentally relevant conditions. This will support scientists and regulators involved in fate modeling and exposure assessment to understand the environmental behavior of (nano)particulate contaminants.

Abbreviations

α_{het}	Heteroagglomeration attachment efficiency
DLS	Dynamic light scattering
DOC	Dissolved organic carbon
LD	Laser diffractometry
ICP-OES	Inductively coupled plasma optical emission spectrometry
mod.SPM	Model flocs
mod.W	Model water
nat.SPM	Natural flocs
nat.W	Natural water
NM	Nanomaterial
NPOC	Non-purgeable organic carbon
SEM	Scanning electron microscopy
SP-ICP-MS	Single particle inductively coupled plasma mass spectrometry
SPM	Suspended particulate matter
SR-NOM	Suwannee River natural organic matter
TDN	Total dissolved nitrogen
TG	Test guideline
ZP	Zeta potential

Author contributions

Helene Walch: conceptualization, data curation, formal analysis, investigation, methodology, project administration, supervision, validation, visualization, writing – original draft. Nada Bašić: investigation, validation, writing – review & editing. Antonia Praetorius: conceptualization, supervision, writing – review & editing. Frank von der Kammer: conceptualization, funding acquisition, supervision, writing – review & editing. Thilo Hofmann: resources, supervision, writing – review & editing.

Conflicts of interest

There are no conflicts to declare.

Acknowledgements

References

1 M. F. Hochella, D. W. Mogk, J. Ranville, I. C. Allen, G. W. Luther, L. C. Marr, B. P. McGrail, M. Murayama, N. P. Qafoku, K. M. Rosso, N. Sahai, P. A. Schroeder, P. Vikesland, P. Westerhoff and Y. Yang, Natural, incidental, and engineered nanomaterials and their impacts on the Earth system, *Science*, 2019, **363**, 1414.

2 A. Barhoum, M. L. García-Betancourt, J. Jeevanandam, E. A. Hussien, S. A. Mekkawy, M. Mostafa, M. M. Omran, M. S. Abdalla and M. Bechelany, Review on Natural, Incidental, Bioinspired, and Engineered Nanomaterials: History, Definitions, Classifications, Synthesis, Properties, Market, Toxicities, Risks, and Regulations, *Nanomaterials*, 2022, **12**, 177.

3 H. Wigger, R. Kägi, M. Wiesner and B. Nowack, Exposure and Possible Risks of Engineered Nanomaterials in the Environment—Current Knowledge and Directions for the Future, *Rev. Geophys.*, 2020, **58**, 1–25.

4 A. Praetorius, N. Tufenkji, K.-U. Goss, M. Scheringer, F. von der Kammer and M. Elimelech, The road to nowhere: equilibrium partition coefficients for nanoparticles, *Environ. Sci.: Nano*, 2014, **1**, 317–323.

5 S. Reynaud, A. Aynard, B. Grassl and J. Gigault, Nanoplastics: From model materials to colloidal fate, *Curr. Opin. Colloid Interface Sci.*, 2022, **57**, 101528.

6 W. J. G. M. Peijnenburg, M. Baalousha, J. Chen, Q. Chaudry, F. Von der Kammer, T. A. J. Kuhlbusch, J. Lead, C. Nickel, J. T. K. Quik, M. Renker, Z. Wang and A. A. Koelmans, A Review of the Properties and Processes Determining the Fate of Engineered Nanomaterials in the Aquatic Environment, *Crit. Rev. Environ. Sci. Technol.*, 2015, **45**, 2084–2134.

7 A. Praetorius, E. Badetti, A. Brunelli, A. Clavier, J. A. Gallego-Urrea, A. Gondikas, M. Hassellöv, T. Hofmann, A. Mackevica, A. Marcomini, W. Peijnenburg, J. T. K. Quik, M. Seijo, S. Stoll, N. Tepe, H. Walch and F. von der Kammer, Strategies for determining heteroaggregation attachment efficiencies of engineered nanoparticles in aquatic environments, *Environ. Sci.: Nano*, 2020, **7**, 351–367.

8 E. M. Hotze, T. Phenrat and G. V. Lowry, Nanoparticle Aggregation: Challenges to Understanding Transport and Reactivity in the Environment, *J. Environ. Qual.*, 2010, **39**, 1909–1924.

9 K. L. Garner and A. A. Keller, Emerging patterns for engineered nanomaterials in the environment: a review of fate and toxicity studies, *J. Nanopart. Res.*, 2014, **16**, 2503.

10 J. A. J. Meesters, W. J. G. M. Peijnenburg, A. J. Hendriks, D. Van de Meent and J. T. K. Quik, A model sensitivity analysis to determine the most important physicochemical properties driving environmental fate and exposure of engineered nanoparticles, *Environ. Sci.: Nano*, 2019, **6**, 2049–2060.

11 N. K. Geitner, J. L. Cooper, A. Avellan, B. T. Castellon, B. G. Perrotta, N. Bossa, M. Simonin, S. M. Anderson, S. Inoue, M. F. Hochella, C. J. Richardson, E. S. Bernhardt, G. V. Lowry, P. L. Ferguson, C. W. Matson, R. S. King, J. M. Unrine, M. R. Wiesner and H. Hsu-Kim, Size-Based Differential Transport, Uptake, and Mass Distribution of Ceria (CeO2) Nanoparticles in Wetland Mesocosms, *Environ. Sci. Technol.*, 2018, **52**, 9768–9776.

12 N. K. Geitner, S. M. Marinakos, C. Guo, N. O'Brien and M. R. Wiesner, Nanoparticle Surface Affinity as a Predictor of Trophic Transfer, *Environ. Sci. Technol.*, 2016, **50**, 6663–6669.

13 C. Svendsen, L. A. Walker, M. Matzke, E. Lahive, S. Harrison, A. Crossley, B. Park, S. Lofts, I. Lynch, S. Vázquez-Campos, R. Kaegi, A. Gogos, C. Asbach, G. Cornelis, F. von der Kammer, N. W. van den Brink, C. Mays and D. J. Spurgeon, Key principles and operational practices for improved nanotechnology environmental exposure assessment, *Nat. Nanotechnol.*, 2020, **15**, 731–742.

14 A. Praetorius, J. Labille, M. Scheringer, A. Thill, K. Hungerbühler and J.-Y. Bottero, Heteroaggregation of Titanium Dioxide Nanoparticles with Model Natural Colloids under Environmentally Relevant Conditions, *Environ. Sci. Technol.*, 2014, **48**, 10690–10698.

15 OECD, *Test No. 318: Dispersion Stability of Nanomaterials in Simulated Environmental Media*, OECD Publishing, Paris, 2017.

16 F. Abdolahpur Monikh, A. Praetorius, A. Schmid, P. Kozin, B. Meisterjahn, E. Makarova, T. Hofmann and F. von der Kammer, Scientific rationale for the development of an OECD test guideline on engineered nanomaterial stability, *NanoImpact*, 2018, **11**, 42–50.

17 A. Praetorius, R. Arvidsson, S. Molander and M. Scheringer, Facing complexity through informed simplifications: a research agenda for aquatic exposure assessment of nanoparticles, *Environ. Sci.: Processes Impacts*, 2013, **15**, 161–168.

18 A. Baun, P. Sayre, K. G. Steinhäuser and J. Rose, Regulatory relevant and reliable methods and data for determining the environmental fate of manufactured nanomaterials, *NanoImpact*, 2017, **8**, 1–10.

19 D. Zhou, A. I. Abdel-Fattah and A. A. Keller, Clay Particles Destabilize Engineered Nanoparticles in Aqueous Environments, *Environ. Sci. Technol.*, 2012, **46**, 7520–7526.

20 J. A. Gallego-Urrea, J. Hammes, G. Cornelis and M. Hassellöv, Coagulation and sedimentation of gold nanoparticles and illite in model natural waters: Influence of initial particle concentration, *NanoImpact*, 2016, **3–4**, 67–74.

21 N. K. Geitner, N. J. O'Brien, A. A. Turner, E. J. Cummins and M. R. Wiesner, Measuring Nanoparticle Attachment Efficiency in Complex Systems, *Environ. Sci. Technol.*, 2017, **51**, 13288–13294.

22 S. Bae, J. J. Lenhart and Y. S. Hwang, The effect of ionic strength, pH and natural organic matter on heteroaggregation of CeO2 nanoparticles with montmorillonite clay minerals, *Environ. Eng. Res.*, 2021, **27**, 210470.

23 X. Li, E. He, M. Zhang, W. J. G. M. Peijnenburg, Y. Liu, L. Song, X. Cao, L. Zhao and H. Qiu, Interactions of CeO2 nanoparticles with natural colloids and electrolytes impact their aggregation kinetics and colloidal stability, *J. Hazard. Mater.*, 2020, **386**, 121973.

24 V. Adam, S. Loyaux-Lawniczak, J. Labille, C. Galindo, M. del Nero, S. Gangloff, T. Weber and G. Quaranta, Aggregation behaviour of TiO2 nanoparticles in natural river water, *J. Nanopart. Res.*, 2016, **18**, 13.

25 O. Oriekhova and S. Stoll, Heteroaggregation of nanoplastic particles in the presence of inorganic colloids and natural organic matter, *Environ. Sci.: Nano*, 2018, **5**, 792–799.

26 O. Oriekhova and S. Stoll, Heteroaggregation of CeO2 nanoparticles in presence of alginate and iron (III) oxide, *Sci. Total Environ.*, 2019, **648**, 1171–1178.

27 J. Wang, X. Zhao, F. Wu, Z. Tang, T. Zhao, L. Niu, M. Fang, H. Wang and F. Wang, Impact of montmorillonite clay on the homo- and heteroaggregation of titanium dioxide nanoparticles (nTiO2) in synthetic and natural waters, *Sci. Total Environ.*, 2021, **784**, 147019.

28 M. C. Surette and J. A. Nason, Nanoparticle aggregation in a freshwater river: the role of engineered surface coatings, *Environ. Sci.: Nano*, 2019, **6**, 540–553.

29 L. E. Barton, M. Therezien, M. Auffan, J.-Y. Bottero and M. R. Wiesner, Theory and Methodology for Determining Nanoparticle Affinity for Heteroaggregation in Environmental Matrices Using Batch Measurements, *Environ. Eng. Sci.*, 2014, **31**, 421–427.

30 K. A. Huynh, J. M. McCaffery and K. L. Chen, Heteroaggregation of multiwalled carbon nanotubes and hematite nanoparticles: Rates and mechanisms, *Environ. Sci. Technol.*, 2012, **46**, 5912–5920.

31 A. R. M. N. Afrooz, I. A. Khan, S. M. Hussain and N. B. Saleh, Mechanistic Heteroaggregation of Gold Nanoparticles in a Wide Range of Solution Chemistry, *Environ. Sci. Technol.*, 2013, **47**, 1853–1860.

32 J. Labille, C. Harns, J.-Y. Bottero and J. Brant, Heteroaggregation of Titanium Dioxide Nanoparticles with Natural Clay Colloids, *Environ. Sci. Technol.*, 2015, **49**, 6608–6616.

33 F. Gottschalk, T. Sun and B. Nowack, Environmental concentrations of engineered nanomaterials: Review of modeling and analytical studies, *Environ. Pollut.*, 2013, **181**, 287–300.

34 L. E. Barton, M. Therezien, M. Auffan, J.-Y. Bottero and M. R. Wiesner, Theory and Methodology for Determining Nanoparticle Affinity for Heteroaggregation in Environmental Matrices Using Batch Measurements, *Environ. Eng. Sci.*, 2014, **31**, 421–427.

35 K. L. Chen and M. Elimelech, Aggregation and Deposition Kinetics of Fullerene (C 60) Nanoparticles, *Langmuir*, 2006, **22**, 10994–11001.

36 K. A. Huynh and K. L. Chen, Disaggregation of heteroaggregates composed of multiwalled carbon nanotubes and hematite nanoparticles, *Environ. Sci.: Processes Impacts*, 2014, **16**, 1371–1378.

37 G. Metreveli, A. Philippe and G. E. Schaumann, Disaggregation of silver nanoparticle homoaggregates in a river water matrix, *Sci. Total Environ.*, 2015, **535**, 35–44.

38 M. Therezien, A. Thill and M. R. Wiesner, Importance of heterogeneous aggregation for NP fate in natural and engineered systems, *Sci. Total Environ.*, 2014, **485–486**, 309–318.

39 H. Walch, A. Praetorius, F. von der Kammer and T. Hofmann, Generation of reproducible model freshwater particulate matter analogues to study the interaction with particulate contaminants, *Water Res.*, 2023, **229**, 119385.

40 W. Wang, J. Y. Howe and B. Gu, Structure and Morphology Evolution of Hematite (α-Fe 2 O 3) Nanoparticles in Forced Hydrolysis of Ferric Chloride, *J. Phys. Chem. C*, 2008, **112**, 9203–9208.

41 R. Salminen, M. J. Batista, M. Bidovec, A. Demetriades, B. De Vivo, W. De Vos, M. Duris, A. Gilucis, V. Gregorauskiene, J. Halamic, P. Heitzmann, A. Lima, G. Jordan, G. Klaver, P. Klein, J. Lis, J. Locutura, K. Marsina, A. Mazreku, P. J. O'Connor, S. Å. Olsson, R.-T. Ottesen, V. Petersell, J. A. Plant, S. Reeder, I. Salpeteur, H. Sandström, U. Siewers, A. Steenfelt and T. Tarvainen, *Geochemical Atlas of Europe. Part 1: Background Information, Methodology and Maps*, Geological Survey of Finland, Espoo, 2005.

42 M. Perdue, *Replenishment of the Reference Suwannee River Natural Organic Matter (NOM)*, 2012.

43 IHSS, Elemental Compositions and Stable Isotopic Ratios of IHSS Samples, **https://humic-substances.org/elemental-compositions-and-stable-isotopic-ratios-of-ihss-samples/**, (accessed 22 January 2020).

44 A. Praetorius, M. Scheringer and K. Hungerbühler, Development of Environmental Fate Models for Engineered Nanoparticles—A Case Study of TiO 2 Nanoparticles in the Rhine River, *Environ. Sci. Technol.*, 2012, **46**, 6705–6713.

45 H. Walch, F. von der Kammer and T. Hofmann, Freshwater suspended particulate matter—Key components and processes in floc formation and dynamics, *Water Res.*, 2022, **220**, 118655.

46 N. W. Green, D. McInnis, N. Hertkorn, P. A. Maurice and E. M. Perdue, Suwannee River natural organic matter: Isolation of the 2R101N reference sample by reverse osmosis, *Environ. Eng. Sci.*, 2015, **32**, 38–44.

47 M. H. Shen, Y. G. Yin, A. Booth and J. F. Liu, Effects of molecular weight-dependent physicochemical heterogeneity of natural organic matter on the aggregation of fullerene nanoparticles in mono- and di-valent electrolyte solutions, *Water Res.*, 2015, **71**, 11–20.

48 S. M. Louie, R. D. Tilton and G. V. Lowry, Effects of Molecular Weight Distribution and Chemical Properties of Natural Organic Matter on Gold Nanoparticle Aggregation, *Environ. Sci. Technol.*, 2013, **47**, 4245–4254.

This journal is © The Royal Society of Chemistry 2024

Environ. Sci.: Nano, 2024, **11**, 588–600 | **599**

49 K. M. Kuhn, E. Neubauer, T. Hofmann, F. von der Kammer, G. R. Aiken and P. A. Maurice, Concentrations and Distributions of Metals Associated with Dissolved Organic Matter from the Suwannee River (GA, USA), *Environ. Eng. Sci.*, 2015, **32**, 54–65.

50 IHSS, Acidic Functional Groups of IHSS Samples, https://humic-substances.org/acidic-functional-groups-of-ihss-samples/, (accessed 12 February 2020).

51 T. Ratpukdi, J. A. Rice, G. Chilom, A. Bezbaruah and E. Khan, Rapid Fractionation of Natural Organic Matter in Water Using a Novel Solid-Phase Extraction Technique, *Water Environ. Res.*, 2009, **81**, 2299–2308.

52 H. Wang, A. S. Adeleye, Y. Huang, F. Li and A. A. Keller, Heteroaggregation of nanoparticles with biocolloids and geocolloids, *Adv. Colloid Interface Sci.*, 2015, **226**, 24–36.

53 J. T. K. Quik, I. Velzeboer, M. Wouterse, A. A. Koelmans and D. van de Meent, Heteroaggregation and sedimentation rates for nanomaterials in natural waters, *Water Res.*, 2014, **48**, 269–279.

54 W. J. G. M. Peijnenburg, M. Baalousha, J. Chen, Q. Chaudry, F. Von der Kammer, T. A. J. Kuhlbusch, J. Lead, C. Nickel, J. T. K. Quik, M. Renker, Z. Wang and A. A. Koelmans, A Review of the Properties and Processes Determining the Fate of Engineered Nanomaterials in the Aquatic Environment, *Crit. Rev. Environ. Sci. Technol.*, 2015, **45**, 2084–2134.

55 G. Šafarek, How fast are rivers?, https://worldrivers.net/2020/03/28/how-fast-are-rivers/#:~:text=A moderately fast river flows,like any other moving vehicle.

56 B. G. Krishnappan, In Situ Size Distribution of Suspended Particles in the Fraser River, *J. Hydraul. Eng.*, 2000, **126**, 561–569.

57 K. L. Priya, P. Jegathambal and E. J. James, On the factors affecting the settling velocity of fine suspended sediments in a shallow estuary, *J. Oceanogr.*, 2015, **71**, 163–175.

58 R. K. Chakraborti, J. F. Atkinson and J. Kaur, Effect of Mixing on Suspended Particle-Size Distribution, *J. Environ. Eng.*, 2009, **135**, 306–316.

59 J. Huang, S. Wang, X. Li, R. Xie, J. Sun, B. Shi, F. Liu, H. Cai, Q. Yang and Z. Zheng, Effects of Shear Stress and Salinity Stratification on Floc Size Distribution During the Dry Season in the Modaomen Estuary of the Pearl River, *Front. Mar. Sci.*, 2022, **9**, 1–18.

60 M. Pejrup and O. A. Mikkelsen, Factors controlling the field settling velocity of cohesive sediment in estuaries, *Estuarine, Coastal Shelf Sci.*, 2010, **87**, 177–185.

61 F. Abdolahpur Monikh, A. Praetorius, A. Schmid, P. Kozin, B. Meisterjahn, E. Makarova, T. Hofmann and F. von der Kammer, Scientific rationale for the development of an OECD test guideline on engineered nanomaterial stability, *NanoImpact*, 2018, **11**, 42–50.

62 A. Philippe and G. E. Schaumann, Interactions of Dissolved Organic Matter with Natural and Engineered Inorganic Colloids: A Review, *Environ. Sci. Technol.*, 2014, **48**, 8946–8962.

63 S. Yu, J. Liu, Y. Yin and M. Shen, Interactions between engineered nanoparticles and dissolved organic matter: A review on mechanisms and environmental effects, *J. Environ. Sci.*, 2018, **63**, 198–217.

64 T. Zhu, D. F. Lawler, Y. Chen and B. L. T. Lau, Effects of natural organic matter and sulfidation on the flocculation and filtration of silver nanoparticles, *Environ. Sci.: Nano*, 2016, **3**, 1436–1446.

65 A. Praetorius, A. Gundlach-Graham, E. Goldberg, W. Fabienke, J. Navratilova, A. Gondikas, R. Kaegi, D. Günther, T. Hofmann and F. von der Kammer, Single-particle multi-element fingerprinting (spMEF) using inductively-coupled plasma time-of-flight mass spectrometry (ICP-TOFMS) to identify engineered nanoparticles against the elevated natural background in soils, *Environ. Sci.: Nano*, 2017, **4**, 307–314.

66 D. M. Mitrano, A. Beltzung, S. Frehland, M. Schmiedgruber, A. Cingolani and F. Schmidt, Synthesis of metal-doped nanoplastics and their utility to investigate fate and behaviour in complex environmental systems, *Nat. Nanotechnol.*, 2019, **14**, 362–368.